Control-Oriented Modelling of Wave Energy Converter M4

Zhijing Liao[#1], Nian Gai[#2], Peter Stansby[*3], Guang Li[#4]
[#]*School of Engineering and Material Science, Queen Mary University of London*
Queen Mary University of London, London, E1 4NS UK
[1]z.liao@qmul.ac.uk
[2]n.gai@qmul.ac.uk
[4]g.li@qmul.ac.uk
[*]*School of Mechanical, Aerospace and Civil Engineering*
University of Manchester, Manchester M13 9PL, UK
[3]p.k.stansby@manchester.ac.uk

***Abstract*—This paper aims to establish a control-oriented state-space model for the M4 wave energy converter for the purpose of controller design. The Euler-Lagrangian equation is used to describe the dynamics of M4 in a unified and concise format. The linear wave radiation damping term is expressed as a state-space subsystem, which is then integrated into a state-space model for the whole device. A model order reduction technique is used to reduce the order of the state-space model. The fidelity of the resulting state-space models with different orders is validated in both frequency domain and time domain. The result of this paper paves the way for the future research on developing model-based controller for M4 device to further improve its energy conversion efficiency. The modeling procedure can be transferred to other types of multi-float multi-motion WECs.**

***Keywords*– Wave energy converter, state-space model, model order reduction.**

I. Introduction

Many different wave energy converters (WECs) have been invented to harness wave energy, ranging from single-float single-motion point absorbers to multi-float multi-motion WECs (MWECs). Besides the development of device design, control is considered as another indispensable approach to further improve the energy conversion efficiency and survivability of WECs [1]. Most early WEC control methods, such as latching control and declutch control, are based on impedance matching principle, that is, maximum energy output can be achieved when the resonance frequency of a WEC is close to the dominant frequency of incoming waves [2].

Recent studies reveal that model-based optimal control strategies developed for WEC control, e.g. noncausal linear optimal control [3], model predictive control (MPC) [4], [5], pseudospectral control [6], [7], can significantly improve WEC operation performance over conventional WEC control strategies. However, the performance of these advanced model-based WEC control methods rely more on the fidelity of the control-oriented WEC models and can be more computationally demanding compared with the conventional WEC control methods, especially for those control methods which need online optimization, e.g. MPC. This explains why most of the existing case studies for these advanced control methods are mainly focused on single float point absorbers, which have much less modeling complexity than MWECs.

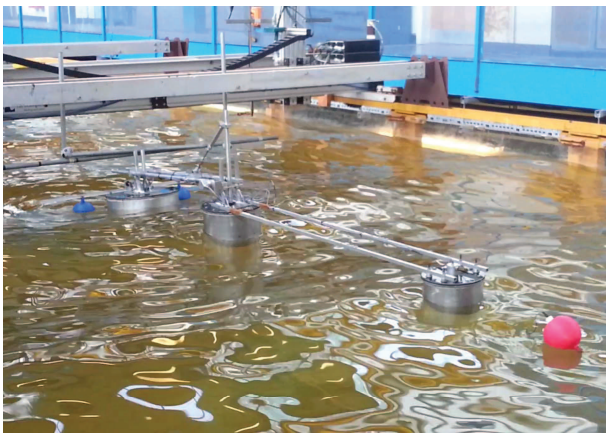

Fig. 1. Tank experiment of M4 in Manchester [8]

Motivated by the fact that model-based optimal control methods can significantly improve performance of single float WECs [1], [9], this paper aims to develop control-oriented models for MWECs with sufficient fidelity but reduced complexities in terms of nonlinearities and the model order, which paves the way for further development of economically implementable model-based advanced control strategies for MWECs. We choose M4 developed in Manchester as a case study, see Fig. 1 for a specific M4 device during tank testing. M4 is a well-designed multi-float multi-motion two-raft-type WEC with reconfigurable structures [8]. Two particular advantages of choosing M4 as a case study are: i) the reconfigurable design of M4, in terms of the number of floats, size, layout etc, brings great convenience for the study of this device with different levels of design complexities; ii) its linear diffraction modelling has been shown to be accurate for both operational and high wave conditions, which makes the control-oriented modeling and the future controller design much less challeng-

ing. M4 has six possible modes and typically three (surge, heave and pitch) are prominent in absorbing wave energy for conversion to electricity and the absorption from each mode are additive. A lot of efforts have been made in the design phase for optimizing the power capture ability of M4 and its conversion efficiency can be potentially further improved by control of its power take-off (PTO). For this purpose, a control-oriented model is the prerequisite and will be developed in this paper from an accurate linear diffraction model proposed in [8].

The rest of the paper is organized as follows. The M4 device and its hydrodynamic model are introduced in Section 2 as well as the control-oriented model. Simulation results are demonstrated and discussed in Section 3. Section 4 concludes this paper and addresses the future work.

II. The M4 device and its hydrodynamic model

A. The M4 device

By changing the number of mid and stern floats, different formats of the device can be built up suitable for different wave conditions. Fig. 2 presents the geometry of a laboratory scale(1:40) three-float M4. From left to right, the bow float, middle float, stern float, beam connecting bow and middle float, beam connecting middle and stern float, and the power take-off (PTO) unit are indexed from 1 to 6, respectively. The M4 with the simplest configuration of type 1-1-1 (indicating the numbers of bow, mid and stern floats respectively) is adopted here for demonstration purpose. Note that the modelling method proposed in this paper can also be used on other formats of the device without lose of generality. With the bow float and mid float connected by a beam to form one rigid body, the stern float connected by a beam to hinge point as another rigid body, the device can rotate about the hinge point when it is aligned to the wave propagating direction. The PTO unit above the hinge point reacts against the body rotation to absorb kinetic energy from incoming waves. Positive directions of displacements are shown in Fig. 2. All rotations are about hinge point O and clockwise positive.

Some useful notations for the following sections are shown in Table I.

TABLE I

Symbol	Description
i	index of each part
r_i	radius of float i
x_i	surge motion of i
z_i	heave motion of i
x_0	surge motion of hinge O
z_0	heave motion of hinge O
θ_1	pitch of i which are on the left of the hinge O
θ_2	pitch of i which are on the right of the hinge O
h_i	horizontal distance from COG of i to hinge O
v_i	vertical distance from COG of i to hinge O
m_i	mass of i, including ballast if its a float
I_i	inertia of i relative to its own COG
ρ	water density
g	gravitational constant

B. M4 Dynamic modelling

An energy-based Lagrangian modelling method is presented in [10] for a two-raft-type wave energy converter. This method is adopted and extended in this paper for the time domain dynamic modelling of the 1-1-1 type M4 with 3 floats. In this section the motion equation is deduced and the process to derive the final state-space model is demonstrated.

The six degrees of freedom (DOF) surge, sway, heave, roll, pitch and yaw of a float are denoted as mode from 1 to 6, respectively. The device is moored from the bow float and it aligns naturally with the wave direction. And roll motion of the device is prevented by outrigger buoys added to the bow float. Then for simplicity and consistency, the concern in this paper will be only motion in x-o-z plane. Therefore, the linear wave forces are also considered only in mode 1, 3 and 5.

The Lagrangian-Euler equation is used to derive the motion equation for this multi-float device with displacement and rotation about the hinge point. First, the generalized coordinate is chosen as $q = [x_0\, z_0\, \theta_1\, \theta_2]^T$. This generalized coordinate is proven to be independent, complete and holonomic to describe the plane motion of the system. Then for each part of the device, the surge and heave motion can be expressed by the generalized coordinate, as shown in (1). Since θ is small, approximations $\sin\theta \approx \theta$ is used in the following coordinate transformation:

$$\begin{aligned} x_1 &= x_0 - v_1\theta_1, \quad z_1 = z_0 + h_1\theta_1 \\ x_2 &= x_0 - v_2\theta_1, \quad z_2 = z_0 + h_2\theta_1 \\ x_3 &= x_0 - v_3\theta_2, \quad z_3 = z_0 - h_3\theta_2 \\ x_4 &= x_0 - v_4\theta_1, \quad z_4 = z_0 + h_4\theta_1 \\ x_5 &= x_0 - v_5\theta_2, \quad z_5 = z_0 - h_5\theta_2 \\ x_6 &= x_0 - v_6\theta_2, \quad z_6 = z_0 - h_6\theta_2 \end{aligned} \tag{1}$$

The dynamics of the M4 device can be expressed by a generic Lagrangian-Euler equation

$$\frac{\mathrm{d}}{\mathrm{d}t}\left(\frac{\partial L}{\partial \dot{q}}\right) - \frac{\partial L}{\partial q} = Q \tag{2}$$

where the Lagrangian $L := T - V$, with T as the total kinetic energy

$$\begin{aligned} T = &\sum_{i=1,2,4}\left[\frac{1}{2}m_i(\dot{x}_i^2 + \dot{z}_i^2) + \frac{1}{2}I_i\dot{\theta}_1^2\right] \\ &+ \sum_{i=3,5,6}\left[\frac{1}{2}m_i(\dot{x}_i^2 + \dot{z}_i^2) + \frac{1}{2}I_i\dot{\theta}_2^2\right] \end{aligned} \tag{3}$$

and V is the total potential energy:

$$V = \sum_{i=1}^{6} m_i g z_i \tag{4}$$

Q is the generalized force acting on the system, and represents the virtual work done by all non-conservative forces when the

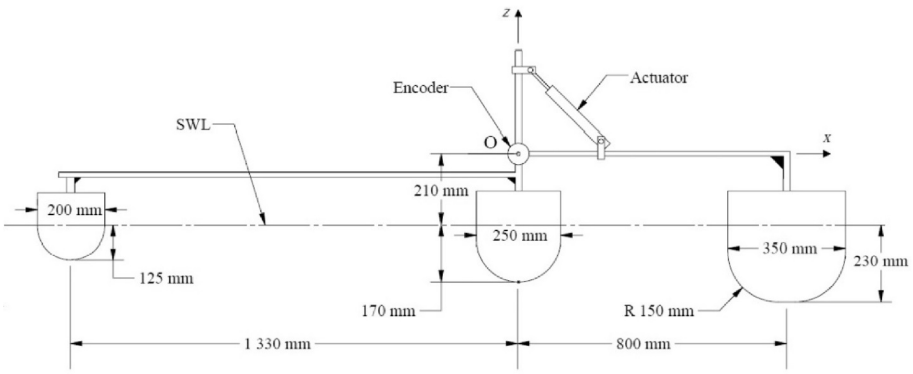

Fig. 2. Diagram of laboratory scale three-float M4 [8]

system is displaced by an infinitesimal value of the generalized coordinate:

$$Q = f_{b,q} + f_{w,q} + f_{pto,q} \tag{5}$$

where $f_{b,q}$ denotes buoyancy force, $f_{w,q}$ denotes linear wave forces, and $f_{pto,q}$ denotes PTO unit moment. Then from the Lagrangian equation, we derive

$$M\ddot{q}(t) + C = f_{b,q}(t) + f_{w,q}(t) + f_{pto,q}(t) \tag{6}$$

Here M is from the kinetic energy derivative, shown in (7). Diagonal terms are summation of mass and inertia with the hinge point O as the reference. Non-diagonal terms account for the coupling dynamics between displacement and rotation. C is from the potential energy derivative, and is expressed by

$$C = \begin{bmatrix} 0 \\ \sum_{i=1}^{6} m_i \\ m_1h_1 + m_2h_2 + m_4h_4 \\ -m_3h_3 - m_5h_5 - m_6h_6 \end{bmatrix} g \tag{8}$$

C indicates the gravity force acting on the system, and it is cancelled by the generalized buoyancy force $f_{b,q}$ at equilibrium [2]. This indicates that all the energy absorbed by the PTO unit comes from the kinetic energy of the system.

According to linear wave theory, the linear wave force $f_{w,q}$ is composed of the excitation force, radiation damping force and hydrostatic restoring force [11], and is denoted by

$$f_{w,q} = f_{e,q} + f_{rd,q} + f_{rs,q} \tag{9}$$

The dynamic equation (6) can now be written as,

$$M\ddot{q}(t) = f_{e,q}(t) + f_{rd,q}(t) + f_{rs,q}(t) + f_{pto,q}(t) \tag{10}$$

We replace the generalized coordinate index q by i,j to denote the forces or torques acting on float i in j mode, with $j = 1, 3, 5$ denoting surge, heave and pitch mode, respectively. Thus, the generalized linear wave forces can be calculated as (11), (12), and (13). Note that all 'f's are functions of time. Linear wave forces act only on floats. Beams and the PTO unit are above the water surface and have no interaction with waves.

C. Hydrodynamic coefficients and linear wave forces

Hydrodynamic coefficients, derived from hydrodynamic software WAMIT, are used to calculate the linear wave forces for each float. The coefficients include excitation force amplitude F_{ex}, excitation force phase ϕ, infinity added mass matrix A_{inf} and radiation damping coefficient $B_{mn}(\omega)$. These forces are calculated as follows:

1) Wave excitation force: Wave excitation force is independent of the system, and it is treated as a disturbance input to the control system. We use the JONSWAP (Joint North Sea Wave Project) wave model to generate irregular wave spectrum with a frequency intervals 200, which is the same as the wave profile used in [8]. Thus, F_{ex} and ϕ are matrices of size 200×18 (here $18 = 3$ floats $\times$ 6 DOFs). The excitation force for float i in mode j is

$$f_{e,i,j} = \sum_{n=1}^{200} H(n) F_{ex}(n, 6(i-1)+j) \cos(\phi(n, 6(i-1)+j) + \phi_{ran}(n)) \tag{14}$$

where $H(n)$ and $\phi_{ran}(n)$ are the amplitude and random phase of JONSWAP wave spectrum, of size 200×1. Substituting all the 'f' terms in (11) by the expression of (14) yields the final generalized excitation force, which is a 4×1 vector.

2) Radiation damping force: Radiation damping force can be expressed by Cummins equation which is a convolution of impulse response function(IRF) and the first derivative of a motion. The IRF L_{mn} is calculated by the radiation damping matrix B_{mn} for m, $n = 1 \ldots 18$,

$$L_{mn}(t) = \frac{2}{\pi} \int_0^\infty B_{mn}(\omega) \cos(\omega t) d\omega \tag{15}$$

Thus the radiation damping force for float i in mode j in time domain can be calculated as,

$$f_{rd,i,j} = \sum_{n=1}^{3} \dot{x}_n * L_{6(i-1)+j,6(n-1)+1}(t) + \sum_{n=1}^{3} \dot{z}_n * L_{6(i-1)+j,6(n-1)+3}(t)$$

$$M = \begin{bmatrix} \sum_{i=1}^{6} m_i & 0 & -m_1v_1 - m_2v_2 - m_4v_4 & -m_3v_3 - m_5v_5 - m_6v_6 \\ 0 & \sum_{i=1}^{6} m_i & m_1h_1 + m_2h_2 + m_4h_4 & -m_3h_3 - m_5h_5 - m_6h_6 \\ -m_1v_1 - m_2v_2 - m_4v_4 & m_1h_1 + m_2h_2 + m_4h_4 & \sum_{i=1,2,4}(I_i + m_i(h_i^2 + v_i^2)) & 0 \\ -m_3v_3 - m_5v_5 - m_6v_6 & -m_3h_3 - m_5h_5 - m_6h_6 & 0 & \sum_{i=3,5,6}(I_i + m_i(h_i^2 + v_i^2)) \end{bmatrix} \tag{7}$$

$$f_{e,q}(t) = \begin{bmatrix} f_{e,1,1} + f_{e,2,1} + f_{e,3,1} \\ f_{e,1,3} + f_{e,2,3} + f_{e,3,3} \\ f_{e,1,5} + f_{e,2,5} - f_{e,1,1}v_1 - f_{e,2,1}v_2 + f_{e,1,3}h_1 + f_{e,2,3}h_2 \\ f_{e,3,5} - f_{e,3,1}v_3 - f_{e,3,3}h_3 \end{bmatrix} \tag{11}$$

$$f_{rd,q}(t) = \begin{bmatrix} f_{rd,1,1} + f_{rd,2,1} + f_{rd,3,1} \\ f_{rd,1,3} + f_{rd,2,3} + f_{rd,3,3} \\ f_{rd,1,5} + f_{rd,2,5} - f_{rd,1,1}v_1 - f_{rd,2,1}v_2 + f_{rd,1,3}h_1 + f_{rd,2,3}h_2 \\ f_{rd,3,5} - f_{rd,3,1}v_3 - f_{rd,3,3}h_3 \end{bmatrix} \tag{12}$$

$$f_{rs,q}(t) = \begin{bmatrix} f_{rs,1,1} + f_{rs,2,1} + f_{rs,3,1} \\ f_{rs,1,3} + f_{rs,2,3} + f_{rs,3,3} \\ f_{rs,1,5} + f_{rs,2,5} - f_{rs,1,1}v_1 - f_{rs,2,1}v_2 + f_{rs,1,3}h_1 + f_{rs,2,3}h_2 \\ f_{rs,3,5} - f_{rs,3,1}v_3 - f_{rs,3,3}h_3 \end{bmatrix} \tag{13}$$

$$+ \sum_{n=1}^{2} \dot{\theta}_1 * L_{6(i-1)+j,6(n-1)+5}(t) + \dot{\theta}_2 * L_{6(i-1)+j,6(n-1)+5|_{n=3}}(t) \tag{16}$$

Here the summation index n refers to each float. Notation '$*$' denotes convolution with upper and lower limits for integration as t and $-\infty$. For example, the portion of radiation damping force acting on float 1 in surge direction caused by the heave motion of float 2 is,

$$f(t) = \int_{-\infty}^{t} L_{1,9}(t-\tau)\dot{z}_2(\tau)d\tau \tag{17}$$

The lower limit can be set to $t - 4T_p$ with sufficient accuracy [8], where T_p is the wave peak period.

Convolution calculation is time-consuming, and there are 81 convolutions in total to be calculated according to the above analysis. Substituting all 'f's in (12) with (16), applying the linear property of convolution and introducing the motions of each float into the generalized variable by (1), we can write the generalized radiation force in a matrix form

$$f_{rd,q}(t) = \int_{t-4T_p}^{t} F_{rd}(t-\tau)\dot{q}(\tau)d\tau \tag{18}$$

where F_{rd} is a 4×4 matrix with an IRF of length $4T_p$ in each entry. $\dot{q}$ is first derivative of the generalized coordinate vector. Now the number of convolutions need to be calculated is reduced to 16.

A state-space model can be derived from each convolution term, as shown in [12]. The Hankel singular value decomposition algorithm is used to convert each convolution term to a state-space model. The order of the model is proportional to the length of the IRF $F_{rd,mn}$ and can be very high; in this case study, it is around 400. Then assembling the 16 converted state-space models into one state-space model with with an order of around 6400×6400, which is too high for model-based control algorithms. Thus, model order reduction is necessary for reducing each state-space model. The truncated balanced reduction method is employed to reduce the originally converted state-space model with an order of around 400 to a model with an order of 3 to 8. System identification and truncated balanced reduction method are implemented using MATLAB routines $imp2ss()$ and $balmr()$, respectively. Order 8 for each subsystem is chosen in this paper for simulation, validation in both time and frequency domain is shown in next chapter.

Now the generalized radiation damping force can be expressed as,

$$\begin{aligned} \dot{z}_s &= A_s z_s + B_s \dot{q}(t) \\ f_{rd,q}(t) &= C_s z_s + D_s \dot{q}(t) \end{aligned} \tag{19}$$

where $\dot{z}_s$ is the state variable of the identified and assembled system with an order of 128 and has no physical meaning. $A_s,\ B_s,\ C_s,\ D_s$ are the state-space representation matrixes. Their sizes are 128×128, 128×4, 4×128, 4×4, respectively.

The added mass matrix A_{inf} when the frequency approaches infinity is of size 18×18, with only a constant value in each entry. The added mass term can be viewed as a force relative to second derivative of the generalized variable, $\ddot{q}(t)$. It can also be added to the matrix M, after reassembled to a 4×4 matrix m_∞ following the same way of radiation damping force in (12), which is adopted here.

3) Hydrostatic restoring force: Hydrostatic restoring force is dependent on the heave displacement and pitch rotation, but not on surge, i.e. $f_{rs,i,1} = 0$. The heave restoring force for float i is $f_{rs,i,3} = -\rho g \pi r_i^2 z_i$, and the pitch restoring torque for

float i is $f_{rs,i,5} = -\rho g \pi \frac{r_i^4}{4} \theta_{1or2}$. From (13), the generalized hydrostatic restoring force can be written in a matrix form

$$f_{rs,q}(t) = Kq(t) \tag{20}$$

where K is the 4×4 hydrostatic restoring force matrix,

$$K = \begin{bmatrix} 0 & 0 & 0 & 0 \\ 0 & \sum_{i=1}^{3} k_{zi} & k_{z1}h_1 + k_{z2}h_2 & -k_{z3}h_3 \\ 0 & k_{z1}h_1 + k_{z2}h_2 & \sum_{i=1}^{2} k_{ri} + k_{zi}h_i^2 & 0 \\ 0 & -k_{z3}h_3 & 0 & k_{r3} + k_{z3}h_3^2 \end{bmatrix} \tag{21}$$

$k_{zi} = -\rho g \pi r_i^2$, $k_{ri} = -\rho g \pi \frac{r_i^4}{4}$ are respectively the restoring coefficients for heave force and pitch moment of float i.

To sum up, the motion equation for M4 can be written as,

$$\begin{aligned} (M + m_\infty)\ddot{q}(t) + f_{rd,q}(t) + Kq(t) &= f_{e,q}(t) + f_{pto,q}(t) \\ \dot{z}_s &= A_s z_s + B_s \dot{q}(t) \\ f_{rd,q}(t) &= C_s z_s + D_s \dot{q}(t) \end{aligned} \tag{22}$$

At the modelling stage, the PTO moment M_{mech} is modelled as $M_{mech} = -B_{mech}\dot{\theta}_r$, where B_{mech} is a constant coefficient and $\dot{\theta}_r := \dot{\theta}_1 - \dot{\theta}_2$ is the relative pitch rotation velocity. However, the generalized PTO force can be viewed as a manipulable control input to the whole system at the controller design stage and takes the form of

$$f_{pto,q}(t) = \begin{bmatrix} 0 \\ 0 \\ -M_{mech}(t) \\ M_{mech}(t) \end{bmatrix} \tag{23}$$

By defining a new state vector $x := [q,\ \dot{q},\ z_s]^T$, the final state-space representation of the M4 control-oriented model can be written as

$$\begin{aligned} \dot{x} &= Ax + Bf_{e,q}(t) + Bf_{pto,q}(t) \\ y &= Cx + Du \end{aligned} \tag{24}$$

where the system matrices are

$$A = \begin{bmatrix} 0_{4\times4} & I_{4\times4} & 0_{4\times n} \\ \frac{-K}{(M+m_\infty)} & \frac{-D_s}{(M+m_\infty)} & \frac{-C_s}{(M+m_\infty)} \\ 0_{n\times4} & B_s & A_s \end{bmatrix} \tag{25}$$

$$B = \begin{bmatrix} 0_{4\times4} \\ (M + m_\infty)^{-1} \\ 0_{n\times4} \end{bmatrix} \tag{26}$$

$$C = \begin{bmatrix} I_{8\times8} & 0_{n\times8} \end{bmatrix} \tag{27}$$

$$D = \begin{bmatrix} 0_{8\times8} \end{bmatrix} \tag{28}$$

with $A \in \mathbb{R}^{136\times136}$ This multi-input-multi-output state-space model has 4 inputs including the wave excitation the manipulable PTO control inputs and 8 outputs which are the generalized motion and its velocity.

III. Validation and Simulation

A. Validation of state-space models with different reduced orders

There are totally 16 subsystems expressed by state-space models, all of which need to be validated. For demonstration purpose, we only present the models for the first and the third diagonal subsystems. We compare the time responses of the original hydrodynamic radiation model and the converted state-space models with different orders in Fig. 3 and Fig. 4. It can be seen from Fig. 3(a) and Fig. 4(a) that for different orders, the state-space models with full order, 20th-order and 8th-order match well with the response of the original IRF. The IRF of the 3rd-order state-space model has an obvious degradation. Fig. 3(b) and Fig. 4(b) illustrate the bode diagrams of the state-space models with different orders; the 3rd-order system has a large variation compared with others at low frequency. Based on this analysis, each subsystem is modelled by a state-space model with an order of 8 to form the final system.

B. Responses to wave excitation forces

The system described in (24) is discretized for simulations in MATLAB. The same wave profile is used for all the models in the simulation. The significant wave height of wave input is $H_s = 0.04$ meter and peak period is 1.8 seconds. The linear PTO moment coefficient is chosen as $B_{mech} = 6$. The number of simulation time steps in one peak period is 200, and each time step is $\delta t = 0.009s$. Simulation time duration is 180 seconds, which is long enough to see the model response.

Linear diffraction model simulation is run using $Fortran$ and the result has good agreement with tank experiment result [8]. Power is calculated as $P(t) = B_{mech}\dot{\theta}_r^2(t)$. Fig. 5 shows that the state-space model reproduces very similar responses for each motion, PTO torque and power to that of the linear diffraction model when the same wave excitation force profile is used. Fig. 6 and Fig. 7 show the relative pitch motion and power for the first 50 seconds, which more clearly demonstrate that the state-space model and the linear diffraction model can produce very close responses for the same wave excitation forces.

IV. Conclusion

In this paper, a control-oriented state-space model is developed for a typical multi-motion multi-float wave energy converter, M4. Energy based Lagrangian-Euler modelling method is adopted to provide a concise and generic mathematical description of the device's dynamics including the coupling among different modes. System identification and model order reduction algorithms are used to derive the state-space models. The resulting state-space models with different orders are validated by comparing the responses in both time domain and frequency domain with those of the original linear diffraction model, which has been experimentally validated. Based on this state-space model, we will develop model-based optimal control strategies for M4 to further improve its energy capture ability.

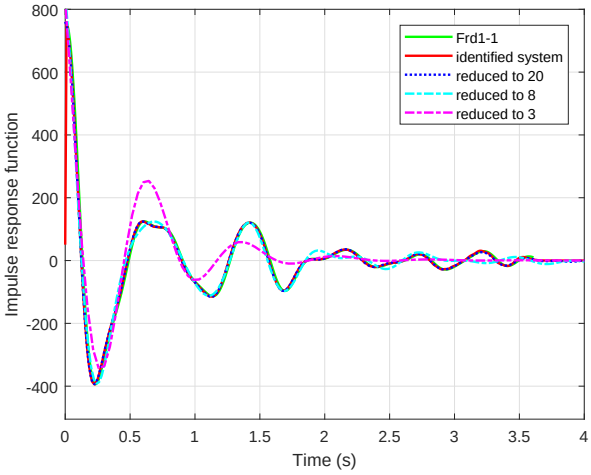

(a) Impulse response function of subsystem $F_{rd,1,1}$

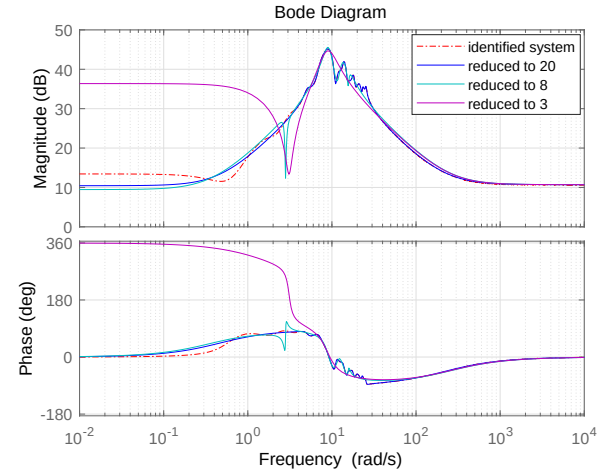

(b) Bode diagram of subsystem $F_{rd,1,1}$

Fig. 3. Validation $F_{rd,1,1}$

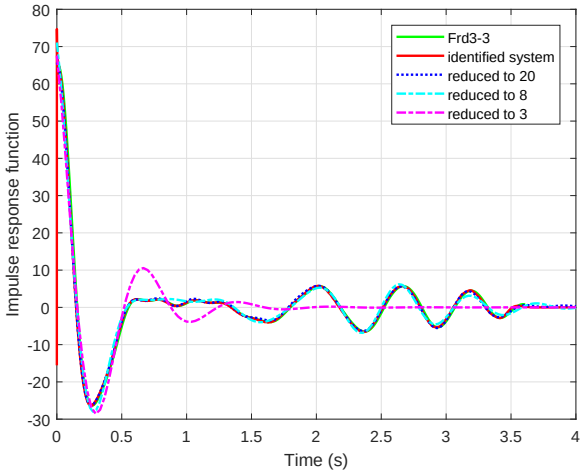

(a) Impulse response function of subsystem $F_{rd,3,3}$

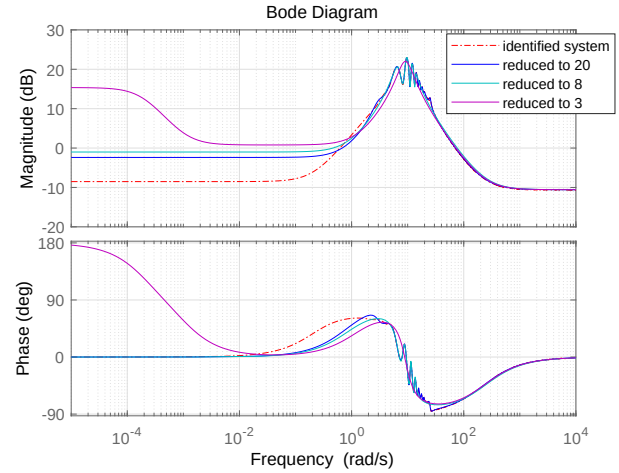

(b) Bode diagram of subsystem $F_{rd,3,3}$

Fig. 4. Validation $F_{rd,3,3}$

ACKNOWLEDGMENT

Zhijing Liao and Nian Gai are grateful to the financial support from the joint "Queen Mary University of London-China Scholarship Council" scholarship.

This work was also supported by Newton Advanced Fellowship (NA160436) by the Royal Society and NSFC.

REFERENCES

[1] J. V. Ringwood, G. Bacelli, and F. Fusco, "Energy-maximizing control of wave-energy converters: The development of control system technology to optimize their operation," *IEEE Control Systems*, vol. 34, no. 5, pp. 30–55, 2014.

[2] J. Falnes, *Ocean Waves and Oscillating Systems: Linear Interactions Including Wave-Energy Extraction*. Cambridge University Press, 2002.

[3] S. Zhan and L. Guang, "Linear noncausal optimal control of wave energy converters," *IEEE Transactions on Control System Technology*, 2018.

[4] G. Li and M. R. Belmont, "Model predictive control of sea wave energy converters–part i: A convex approach for the case of a single device," *Renewable Energy*, vol. 69, pp. 453–463, 2014.

[5] S. Zhan, W. He, and G. Li, "Robust feedback model predictive control of sea wave energy converters," *IFAC-PapersOnLine*, vol. 50, no. 1, pp. 141 – 146, 2017, 20th IFAC World Congress. [Online]. Available: http://www.sciencedirect.com/science/article/pii/S2405896317300368

[6] G. Li, "Nonlinear model predictive control of a wave energy converter based on differential flatness parameterisation," *International Journal of Control*, vol. 90, no. 1, pp. 68–77, 2017.

[7] R. Genest and J. V. Ringwood, "A critical comparison of model-predictive and pseudospectral control for wave energy devices," *Journal of Ocean Engineering and Marine Energy*, vol. 2, no. 4, pp. 485–499, 2016.

[8] P. Stansby, E. C. Moreno, and T. Stallard, "Large capacity multi-float configurations for the wave energy converter m4 using a time-domain linear diffraction model," *Applied Ocean Research*, vol. 68, pp. 53 – 64, 2017. [Online]. Available: http://www.sciencedirect.com/science/article/pii/S0141118717302146

[9] G. Li, G. Weiss, M. Mueller, S. Townley, and M. R. Belmont, "Wave energy converter control by wave prediction and dynamic programming," *Renewable Energy*, vol. 48, pp. 392–403, 2012.

[10] C. Liu, Q. Yang, and G. Bao, "Performance investigation of a two-raft-type wave energy converter with hydraulic power take-off unit," *Applied Ocean Research*, vol. 62, no. Complete, pp. 139–155, 2017.

[11] Z. Yu and J. Falnes, "State-space modelling of a vertical cylinder

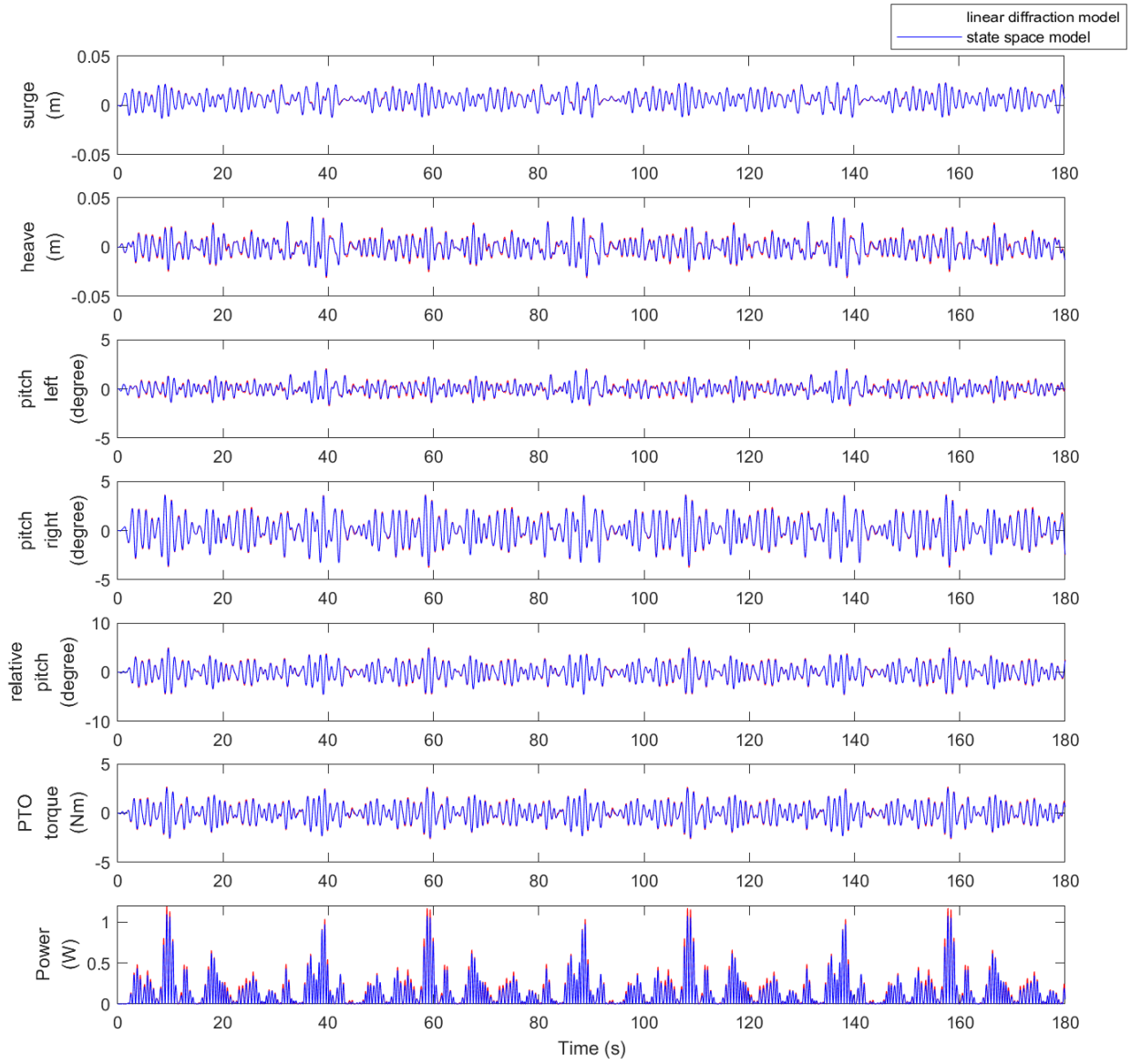

Fig. 5. Comparison of the motions, PTO torque and power for the linear diffraction model and the converted state-space model.

in heave," *Applied Ocean Research*, vol. 17, no. 5, pp. 265 – 275, 1995. [Online]. Available: http://www.sciencedirect.com/science/article/pii/0141118796000028

[12] E. Kristiansen, smund Hjulstad, and O. Egeland, "State-space representation of radiation forces in time-domain vessel models," *Ocean Engineering*, vol. 32, no. 17, pp. 2195 – 2216, 2005. [Online]. Available: http://www.sciencedirect.com/science/article/pii/S0029801805000946

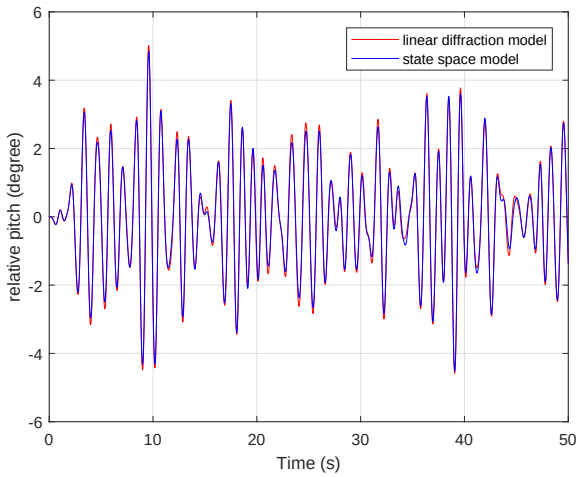

Fig. 6. A comparison of relative pitch motion of the state-space model and that of the linear diffraction model for 50 seconds.

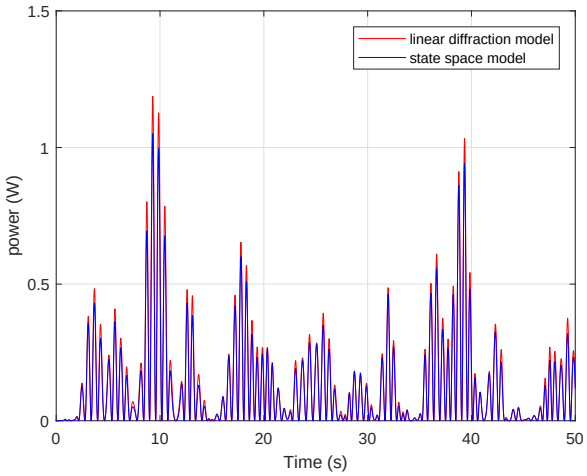

Fig. 7. A comparison of the power outputs from the state-space model and the linear diffraction model for 50 seconds.